Direct measurement of crosswinds to remotely sense 3-D wind-velocity vectors

Devon G. Crowe*,[1] Mark A. Neifeld,[2,3] Jaime A. Anguita,[4] and Anthony D. Gleckler[5]

[1]*Raytheon Company, Space and Airborne Systems*
El Segundo, CA 90245 USA
[2]*Department of Electrical and Computer Engineering, University of Arizona*
[3]*College of Optical Sciences, University of Arizona,*
Tucson, AZ 85721 USA
[4]*College of Engineering and Applied Sciences*
University of the Andes, Santiago 7620001, Chile
[5]*GEOST, 7616 N La Cholla Blvd., Tucson, AZ 85741 USA*

**Corresponding author: devon@raytheon.com*

1. Introduction

We present a method for directly measuring the local 3-D wind-velocity vector using normal 1-D Doppler combined with a range-resolved crosswind measurement that is performed by tracking the displacement of atmospheric turbulence cells over time. Previous work on measuring crosswinds has either used modelling based solely on lidar Doppler wind measurement along the line of sight for a large set of directions of regard [1], or provided passive path-integrated observations of crosswind [2, 3]. A pattern of Shack-Hartman spots that defines the signature of the atmospheric turbulence cells is used to determine its shift due to cross-wind [14], and the angle of rotation is used to determine range using a CGH vortex method.

2. System Description

The proposed system considers a 0.35-μm wavelength, rather than the more common choice of 1.5 μm to measure crosswinds in each range bin [4]. Our choice of wavelength lies in an eyesafe region of the spectrum and offers a large increase in atmospheric return over the common choice mentioned above, as well as a much smaller atmospheric coherence length. These advantages allow using less laser power and smaller optics. In addition, we have chosen an optical vortex (axial rotation) method for range binning, which reduces the computational requirements and eliminates the need for field-programmable gate array (FPGA) control of fast electronics. This reduces electronics cost, power and complexity. The matrix of possible approaches to wind vector measurement using atmospheric turbulence characterization is shown in Table 1.

Table 1. Measurement techniques.

	Time domain	**Space domain**
Image plane	Temporal correlation	Target image motion
Pupil plane	Temporal correlation	Wavefront motion

A wavefront sensor for the spatial domain pupil plane data collection case is shown in Fig.1. A horizontal path through the atmosphere contains significant thermal cell turbulence that perturbs optical wavefront propagation [5, 6]. Measuring the higher order wavefront perturbations characterizes the atmospheric composition at each range [7]. The two-way laser detection and ranging (LIDAR) path self-compensates for global tilts, but the higher-order distortions are still present. A wavefront sensor monitor may be used for multiple range gated exposures to determine the movement of atmospheric turbulence [8]. Target reflection systems are not easily range-gated, implying the need for an aerosol/molecular reflection approach. At each range we sense the combined motion due to all ranges up to the range gate. The motion in a single range bin N is obtained by referencing it to the previous range bin $N - 1$. The laser light is reflected from a combination of the aerosols plus Rayleigh scattering plus thermal cells in each range bin.

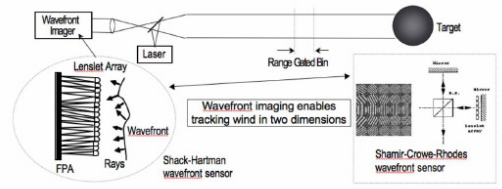

Figure 1. Wavefront measurement.

The axial rotation method of range binning employs a rotating beam for providing the required axial encoding. The rotation is provided by an optical computer-generated hologram (CGH) [9]. Figure 2(a) depicts the notion of a rotating beam. The CGH is conceptually designed to produce a non-symmetric intensity profile that varies in a regular way as a function of propagation distance. In this case we have imposed a two-dot pattern that rotates with propagation [9]. In this way, the round-trip distance experienced by the beam is encoded as a specific value of rotation angle. Figure 2 (b) depicts an example of possible images obtained from reflections at several different distances and in the absence of turbulence. These images can be easily decomposed by filtering on specific values of the rotated beam profile. Figure 2(c) illustrates that a single time exposure over the duration of the round trip to the target contains range bin data encoded by clock angle.

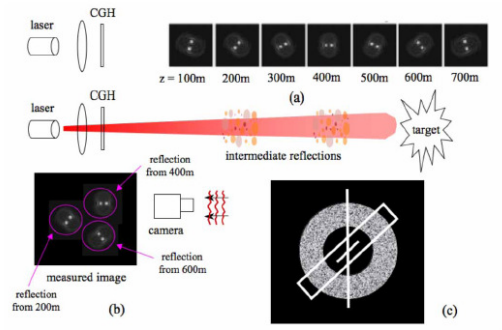

Figure 2. Optical vortex range binning.

Temporal fluctuations associated with turbulent propagation are included within our model by use of the frozen index approximation [10]. Gaussian beam wavefront propagation simulation was performed using the split-step Fourier method [11]. Turbulence was included via the use of random phase screens [12]. To generate the random screens we used a modified version of the Kolmogorov refractive-index power spectrum proposed by Andrews [5]. Another technique for the extraction of wind velocity parameters exploits measurements with high spatial resolution and low temporal resolution. View (a) of Fig. 3 depicts a notional system in which a continuous-wave (CW) probe laser illuminates a target. A mono-static configuration with a 2 cm aperture is used to ensure compactness of the overall deployed system. Reflected light from the target experiences distortion as a result of turbulent propagation. Examples of distorted images obtained from a uniform target at a range of 1 km and under various turbulence conditions are shown in Fig. 3 (b) through (d).

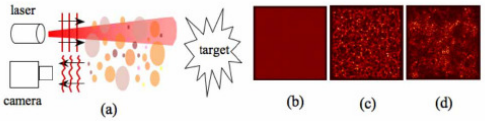

Figure 3. Crosswind measurement system and simulated data.

For small values of wind speed, a simple correlation-based algorithm can be used to estimate wind velocity from a pair of such images. View (a) of Fig. 4 shows a pair of such images separated by 30 ms. Although is it not visually obvious that these two images are related by a simple shift, the correlation pattern shown in Fig. 4(b) verifies this relationship. The graph in Fig. 4(c) shows some initial results obtained using $C^2_n = 10^{-13}$ $m^{-2/3}$. We see that for wind velocities below 1 m/s, this method can be effective. Scaling this simple method to higher wind speeds will require proportional increases in frame rate.

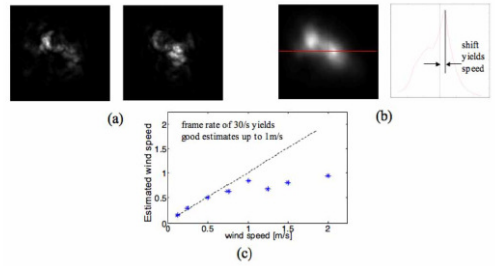

Figure 4. Turbulence images.

We can also extract wind velocity parameters using the measurement of high-resolution temporal data at relatively few spatial locations. A notional system is depicted in Fig. 5(a). Each high-speed photodetector in this arrangement will produce a high-bandwidth signal that carries information about the motion of turbulent eddies throughout the propagation volume. A simple power spectral analysis of this data will yield the desired wind speed estimates. Example power spectra for several values of wind speed are shown in Fig. 5 (b) and (c).We see several features of these power spectra that are well-correlated to aggregate wind speed; the indicated peaks from the 2 ms data are seen to simply scale by

a factor of 5× to yield the 10 ms data. It is important to note that this solution uses an essentially instantaneous measurement of wind speed. This technique will be superior to the multi-frame approach described in the previous section because the multi-frame approach relies on the assumption that index-shift generates image-shift — an assumption that can break down at high wind speed.

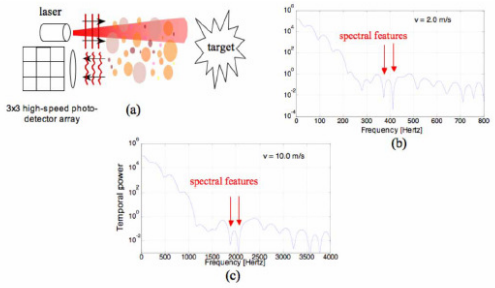

Figure 5. High resolution temporal data.

The wavefront sensor technology for the spatial domain pupil plane data collection case was shown previously in Fig. 1. A horizontal path through the atmosphere contains significant thermal cell turbulence that perturbs optical wavefront propagation [13]. The wavefront at the sensor is effected by turbulence in each range bin. Measuring the higher order wavefront perturbations characterizes the atmospheric composition at each range. Two-way lidar path self-compensates for global tilts, but the higher orders are present. A wavefront sensor monitor is used for multiple range gated exposures to determine the movement of atmospheric turbulence. Target reflection systems are not easily range gateable, implying the need for an aerosol/molecular reflection system. At each range we sense the combined motion due to all ranges up to the range gate. The wind within a single cell is obtained by subtracting the effect of the winds closer than the gate. The laser is reflected from a combination of the aerosols and Rayleigh scattering and thermal cells in each range bin. A crosswind translates the Shack-Hartman wavefront image between measurements (Fig. 6).

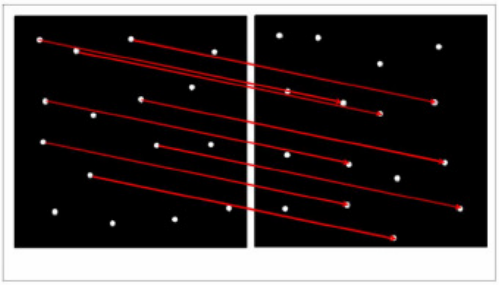

Figure 6. Wavefront displacement with time.

This creates a set of crosswind measurement vectors that should all agree (Fig. 7).

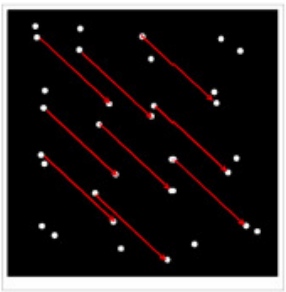

Figure 7. Wavefront data analysis.

Since we know the physical distance the atmosphere traveled between measurements, and the time elapsed between measurements, then we have the velocity as well. The wavelength of operation is selected to maximize each criterion while remaining eye safe. We wish to: minimize laser energy requirements, maximize atmospheric aerosol and molecular scatter signals, and minimize size of the optics. A wavelength of 0.35 μm has several advantages for this application. The backscatter signal from the atmosphere is 100 times stronger than it is at 1.5 μm, and the size of the atmospheric coherence length is 6 times smaller than it is at 1.5 μm, allowing much more compact optics. While the safe threshold is not as high at 0.35 μm as it is beyond 1.5 μm, we can still operate. Examination of the variability in aerosol backscatter using MODTRAN (Fig. 8) reveals that shorter range bins can be sampled when aerosols are denser. Under almost aerosol-free conditions, 50-m range binning may be a good choice. Under optically thick aerosol conditions, 10 meter or smaller bins are supported by the return signal strength. The measurement time in combination with the battery life may dominate the range bin width selection process.

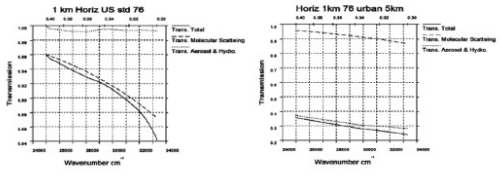

Figure 8. Atmospheric transmission.

3. Conclusion

A method for directly measuring the local 3-D wind-velocity vector using 1-D Doppler wind range component measurements combined with a set of range-resolved crosswind

measurements has been created [14]. Direct measurement of crosswind eliminates the need for approximating crosswinds from a large data set of range-only Doppler wind measurements. This not only reduces the computational load and lowers the modeling error: it also allows performing crosswind measurements along a single line of sight, which enables new applications.

4. Acknowledgements

We thank Rafael Piestun for his rotating-beam example figures and William R. Owens for performing MODTRAN calculations.

5. References

1. F. Durst, B. M. Howe, and G. Richter "Laser-Doppler measurement of crosswind velocity," Appl. Opt. **21**, (1982)
2. S. F. Clifford, G. R. Ochs, and T-i. Wang, "Optical wind sensing by observing the scintillations of a random scene," Appl. Opt. **14**, December (1975).
3. R. Barakat and T. E. Buder, "Remote sensing of crosswind profiles using the correlation
slope method," J. Opt. Soc. Am. **69**, November (1979).
4. S. D. Mayor and S. M. Spuler, "Raman-shifted eye-safe aerosol lidar," Appl. Opt. **43**, 3915–3924 (2004).
5. L. C. Andrews, "An analytical model for the refractive index power spectrum and its application to optical scintillations in the atmosphere," J. Modern Optics **39**, 1849–1853 (1992).
6. L. C. Andrews, M. A. Al-Habash, C. Y. Hopen, R. L. Phillips, "Theory of optical scintillation:
Gaussian-beam wave model," Waves in Random Media **11**, 271–291 (2001).
7. J. Shamir, D. G. Crowe, and J. W. Beletic, "Improved compensation of atmospheric turbulence effects by multiple adaptive mirror systems," App. Opt. **32**, 4618–4628 (1993).
8. Y. Baharav, B. Spektor, J. Shamir, D. G. Crowe,W. Rhodes, and R. Stroud, "Wave-front sensing by pseudo-phase-conjugate interferometry," App. Opt., **34**, 108-113 (1995).
9. A. Greengard, Y. Y. Schechner, and R. Piestun, "Depth from Diffracted Rotation," Opt. Lett. **31**, 181–183 (2006).
10. L. C. Andrews and R. Phillips, *Beam propagation in random media*, 3rd ed., SPIE (2005).
11. A. Belmonte, "Feasibility study for the simulation of beam propagation: consideration of coherent lidar performance," Appl. Opt. **39**, 5426–5445, (2000).
12. J. A. Anguita, M. A. Neifeld, and B. V. Vasic, "Spatial correlation and irradiance statistics in a multiple-beam terrestrial free-space optical communication link," Appl. Opt. **46**, (2007).
13. D. G. Crowe (editor), *Adaptive Optics and Speckle Imaging*, SPIE (1994).
14. D. G. Crowe, U.S. Patent No. 7,705,971, SYSTEM AND METHOD FOR DETERMINING CROSSWINDS.